IOPscience iopscience.iop.org

Home Search Collections Journals About Contact us My IOPscience

Defect pool model based transient photoconductivity and the conduction band tail profile in a-Si:H

This article has been downloaded from IOPscience. Please scroll down to see the full text article.

2001 J. Phys.: Condens. Matter 13 10969

(http://iopscience.iop.org/0953-8984/13/48/321)

View the table of contents for this issue, or go to the journal homepage for more

Download details:
IP Address: 171.66.16.238
The article was downloaded on 17/05/2010 at 04:37

Please note that terms and conditions apply.

INSTITUTE OF PHYSICS PUBLISHING JOURNAL OF PHYSICS: CONDENSED MATTER

J. Phys.: Condens. Matter **13** (2001) 10969–10977 PII: S0953-8984(01)27133-1

Defect pool model based transient photoconductivity and the conduction band tail profile in a-Si:H

A Merazga[1], A F Meftah[1], A M Meftah[1], C Main[2] and S Reynolds[2]

[1] Faculty of Science and Engineering, University Mohamed Khider, BP 145, Biskra 07000, Algeria
[2] School of Science and Engineering, University of Abertay Dundee, Bell Street, Dundee DD1 1HG, UK

E-mail: merazga_amar@hotmail.com

Received 24 July 2001, in final form 25 October 2001
Published 16 November 2001
Online at stacks.iop.org/JPhysCM/13/10969

Abstract

The energy profile of the density of states (DOS) over the mobility gap is determined jointly by the defect pool model (DPM) calculation and the Fourier transform of the transient photoconductivity (TPC), for intrinsic and phosphorus (P)-doped a-Si:H. From the Fourier transform of the TPC, we measure, as a doping effect, an increase of the DOS around the donor energy level, at about 0.16 eV below the conduction mobility edge, and a decrease of the tail width below this level from 21 to 15 meV. This disorder effect on the conduction band tail caused by the P dopant is consistent with the induced doping changes in the dangling bond defect distribution calculated by the DPM. TPC decays are then generated by numerical simulation using this DOS distribution and compared to experimental TPC data. All observed features in the transient photoresponse are reproduced by the simulation, namely the short time rapid decrease followed by the long power law decay in the intrinsic a-Si:H, and the long non-dispersive flat region in the P-doped a-Si:H.

1. Introduction

The defect pool model (DPM) was developed following many attempts to explain the defect formation and calculate the associated energy distribution in a-Si:H. The mechanism was identified as a conversion of weak bonds to dangling bonds [1, 2] and hydrogen diffusion through defects was included as part of such a mechanism [3]. The defect density of states (DOS) distribution was determined [4, 5] using a simple chemical equilibrium description between weak bond energy levels in the valence band tail and energy levels in the gap where the defect is expected to be formed. This DPM was later extended to include the hydrogen energy contribution, either through the related entropy [6] or, otherwise, using the effective mobile hydrogen energy [7]. It is, in fact, this last version of the DPM that we shall adopt

 © 2001 IOP Publishing Ltd Printed in the UK

for the defect density calculation. On the other hand, whereas the valence band tail states are assumed to have an exponential distribution for the defect DOS calculation, the conduction band tail states are ignored in the DPM description. We must, therefore, seek other methods for the determination of the conduction band tail states distribution to cover the whole gap DOS. An exponential distribution of tail states is frequently assumed to occur as a result of structural disorder.

In this paper, we use the transient photoconductivity (TPC) Fourier transform technique [8] to probe the energy distribution of localized state density in the conduction band tail of intrinsic and phosphorus (P)-doped a-Si:H specimens from their TPC responses. We then invoke the DPM and assume an exponential valence band tail to calculate the dangling bond defect DOS using the version in which the capture and release of hydrogen atoms by weak Si–Si bonds are responsible for the defect creation [7]. The resulting DOS with three components of different state types (the valence band donor-like tail states, the conduction band acceptor-like tail states and the dangling bond equivalent one-electron states) is used for modelling the TPC response. It is shown, through comparison with the experimental TPC curves at different temperatures, that the doping-induced changes in the distribution of the conduction band tail states, as determined by the TPC Fourier transform technique, are consistent with the DOS of the dangling bond states calculated by the DPM.

2. Experimental methods

The doped sample was prepared by RF glow discharge decomposition of SiH_4 with 3 vppm PH_3. Coplanar Al electrodes of 0.5 mm gap and 5 mm width were deposited on top of the film of 1 μm thickness, and the voltage applied across the gap was 400 V (i.e. an electric field of 8000 V cm^{-1}). For the intrinsic sample, 0.7 μm thick, the Al electrodes were interdigitated giving an effective conduction cross section of 1.4×10^{-5} cm^2, and the applied electric field was 1.7×10^4 V cm^{-1}. The light source employed was a Laser Science VSL337 N_2-pumped 5 ns pulse dye laser, 640 nm, producing pulsed carrier densities of up to 10^{20} cm^{-3}, varied by means of neutral density filters. Single shots or low frequency ($<$1 Hz) laser pulses were used to allow complete carrier relaxation. The TPC signal was amplified where necessary, and measured using a PC-controlled Tektronix TDS380 oscilloscope as a transient recorder. A temperature range from 120–400 K was covered using a cryostat operating at a chamber pressure of typically 10^{-4} Torr. The dark Fermi level was estimated from the dark conductivity measurement to be 0.75 and 0.50 eV below the conduction band mobility edge for the intrinsic sample and the doped sample, respectively.

3. Simulation methods

The energy profile of the conduction band tail was determined by means of the Fourier transform technique [8, 9]. In essence, this makes use of the fact that the frequency domain photoconductive response of a multiple-trapping system can be related directly to the DOS, in contrast to the time domain or transient response, which in general is a complex function of capture, emission and recombination dynamics. The frequency domain analysis results, after some approximations, in the expression

$$g\left(E_{\omega}\right)=\frac{2}{\pi k_{\mathrm{B}} T C_{n}}\left(\frac{q \mu N \ \sin(\varphi(\omega))}{\left|\hat{\sigma}_{ph}(\omega)\right|}-\omega\right) \tag{1}$$

where q, μ, N and C_n are the electron charge, mobility, pulse density and capture coefficient, respectively. T is the measurement temperature and k_B is the Boltzmann constant. ω is the

effective excitation frequency. The probed energy scale E_ω is determined by the relation $E_\omega = E_c - k_B T \ln(\nu/\omega)$, with ν the attempt to escape frequency. $\left|\hat{\sigma}_{ph}(\omega)\right|$ and $\varphi(\omega)$ are the frequency domain amplitude and phase given by the TPC Fourier transform.

As for the remaining DOS in the gap (the valence band tail and the dangling bond band states), we use the improved DPM described by Powell and Deane [7]. In this approach, the occupancy by hydrogen was defined so that a weak SiSi bond can capture or release one or two hydrogen atoms according to the chemical reactions (2) and (3) below. The bonds SiHD and SiHHSi are, respectively, the dangling bond defect formed at a certain gap energy level and a doubly occupied typical bond created in the valence band:

$$\mathrm{SiHD} \Leftrightarrow \mathrm{SiSi} + \mathrm{H} \tag{2}$$

$$\mathrm{SiHHSi} \Leftrightarrow \mathrm{SiSi} + 2\mathrm{H}. \tag{3}$$

The law of mass action applied to both reactions within the framework of the DPM [6] leads to the following defect states density expression:

$$D(E) = \gamma \left(\frac{2}{f^o(E)}\right)^{k_B T/2E_{vo}} P\left(E + \frac{\sigma^2}{2E_{vo}}\right) \tag{4}$$

with

$$\gamma = \left(\frac{G_V 2E_{vo}^2}{(2E_{vo} - k_B T)}\right)\left(\frac{H}{N_{\mathrm{SiSi}}}\right)^{k_B T/4E_{vo}} \exp\left(\frac{-1}{2E_{vo}}\left(E_P - E_v - \frac{\sigma^2}{4E_{vo}}\right)\right).$$

In equation (4), $P(E)$ is the defect pool of a Gaussian form with σ and E_p its width and peak position in the gap, respectively. G_v and E_{vo} are, respectively, the states density at E_v and the width of the exponential valence band tail. H is the total hydrogen concentration present in pairs in the SiHHSi species, and N_{SiSi} is the total electron concentration in the material. $f^0(E)$ is the occupation function of the neutral dangling bond states.

These DOS components form the electronic structure model for the TPC simulation. The latter is performed according to a finite difference technique [10], where the conduction band tail and valence band tail states are treated as acceptor- and donor-like states, respectively, and the equivalent one-electron DOS is used for the divalent dangling bond states [11]:

$$g_d(E) \approx D(E + k_B T \ln 2) + D(E - U - k_B T \ln 2). \tag{5}$$

This is divided into electron traps above the dark Fermi level E_F with the electron capture coefficient C_{nd}^- much greater than the hole capture coefficient C_{nd}^+, and hole traps below E_F with the hole capture coefficient C_{pd}^+ much greater than the electron capture coefficient C_{pd}^-. The E_F position in the gap is determined prior to the TPC simulation by considering the charge neutrality, involving all free and trapped charges. The charge neutrality condition is maintained at each instant throughout the simulation.

4. Results and discussion

Figure 1 shows a set of six TPC decays for the intrinsic sample at 155, 190, 225, 260, 293 and 330 K measured with an excitation density of 2×10^{14} cm^{-3}. Figure 2 shows a contrasting set of five TPC decays for the doped sample at 150, 200, 250, 290 and 310 K measured with an excitation density of 10^{16} cm^{-3}. Although data in both figures are shown from 10^{-10} s onwards it should be borne in mind that, since the laser pulse is some 5 ns in width, the decay does not accurately reflect multiple trapping processes for times less than about 10^{-8} s. The differences between the two sets of curves are clear. While the intrinsic curves drop at short times (1–10 ns for 330 K) to reflect the deep trapping process [12], the doped sample

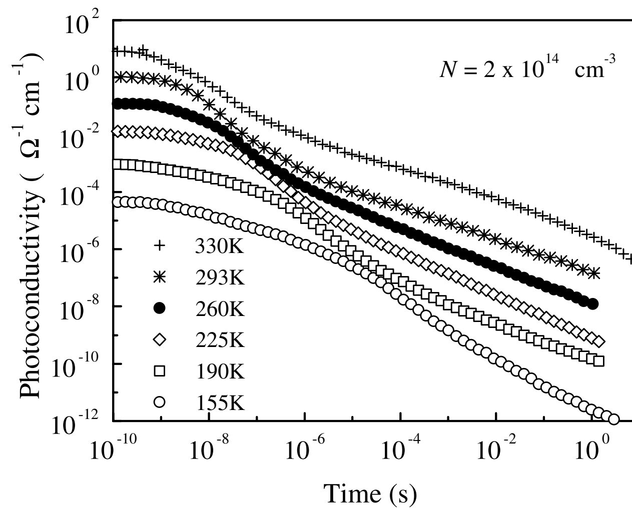

Figure 1. Measured TPC decays for the intrinsic sample at six different temperatures (155, 190, 225, 260, 293 and 330 K) with an excitation density of $N = 2 \times 10^{14}$ cm^{-3}. The curves are offset vertically for clarity.

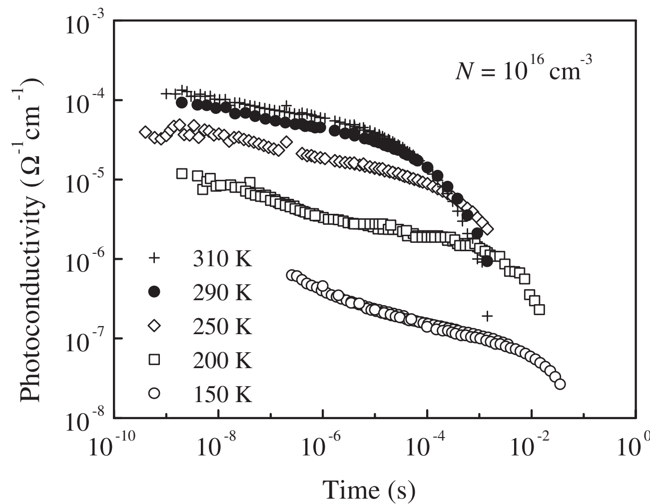

Figure 2. Measured TPC decays for the P-doped sample at five different temperatures (150, 200, 250, 290 and 310 K) with an excitation density of $N = 10^{16}$ cm^{-3}.

curves continue decreasing with very small slopes, indicating non-dispersive transport around a certain shallow energy level [13]. The intrinsic curves present a long approximately power law region between the deep trapping and the recombination regions, but the doped curves show no intermediate transport between the non-dispersive and recombination regions. In both sets of curves, the thermalization processes become slower with decreasing temperature, and the corresponding TPC features shift towards longer times as a result.

The DOS distributions in the conduction band tail as determined by the Fourier transform technique for the intrinsic sample (symbol ○) and the doped sample (symbol $*$) are shown in

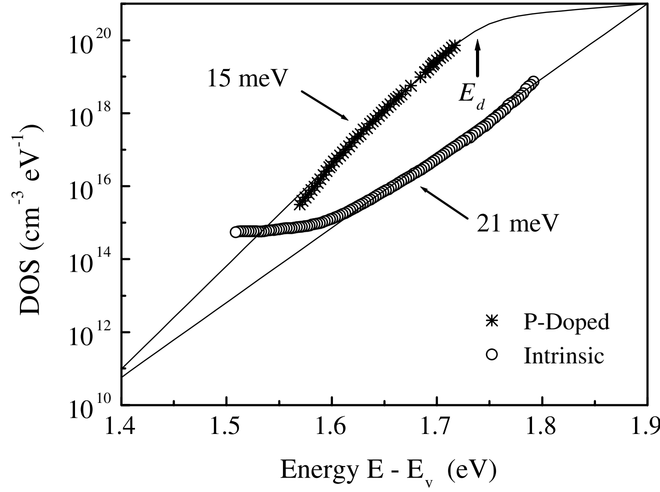

Figure 3. Computed DOS by the Fourier transform of the intrinsic (155 K) TPC (o) and the P-doped (150 K) TPC ($*$) signals. The full curves are the conduction band tail DOS models obtained by fitting with an exponential tail for the intrinsic case and with equation (6) for the doped case. E_d denotes the donor band position.

Table 1. Parameters used for the DOS determination by the TPC Fourier transform technique.

μ (cm^2 s^{-1} V^{-1})	10
C_n (cm^3 s^{-1})	2×10^{-8}
ν (s^{-1})	10^{12}

figure 3. Here, the lowest temperature TPC curves (155 K for intrinsic and 150 K for doped) are chosen to avoid overestimation of the actual DOS by the approximate DOS expression (1) [14]. The parameters used to perform the DOS analysis are given in table 1.

An exponential tail of width approximately 21 meV is obtained for the intrinsic case. For the purposes of comparison the tail is extrapolated to a value $G_c = 10^{21}$ cm^{-3} eV^{-1} at the mobility edge E_c. This tail bends towards deeper energies at the bottom to show a minimum situated around the level 0.4 eV below E_c with a DOS of about 10^{15} cm^{-3} eV^{-1}. The doping effect on the tail shape is remarkable; the DOS with energies around the donor band peak at a certain level E_d between 0.1–0.2 eV below E_c [15] is found to increase with doping. The net result is then, a broad distribution above E_d and a narrow tail below it, so that the conduction band tail profile can be fitted with the DOS model:

$$g_c(E) = G_c \exp\left(\frac{E}{k_B T_{c1}}\right) \Big/ \left(1 + \exp\left(\frac{E_d - E}{k_B T_{c2}}\right)\right) \tag{6}$$

suggesting a tail form with two different slopes, one above E_d with high characteristic temperature T_{c1} and the other below E_d with low characteristic temperature $T_c = T_{c1}T_{c2}/(T_{c1} + T_{c2})$. Least squares fitting gives $E_d = 0.16$ eV below E_c, $T_{c1} = 2143$ K and $T_{c2} = 194$ K, resulting in $T_c \approx 178$ K.

In a previous paper [16], we stated that this tail width ($\sim$15 meV) is extremely low and is due to a doping disorder effect on the tail form occurring around the donor level. We further predicted that this doping effect is in qualitative agreement with the DPM since the latter predicts a low DOS at the tail minimum. Figure 4 shows the complete DOS distributions for the intrinsic and doped cases, including the conduction band tail profiles determined by TPC.

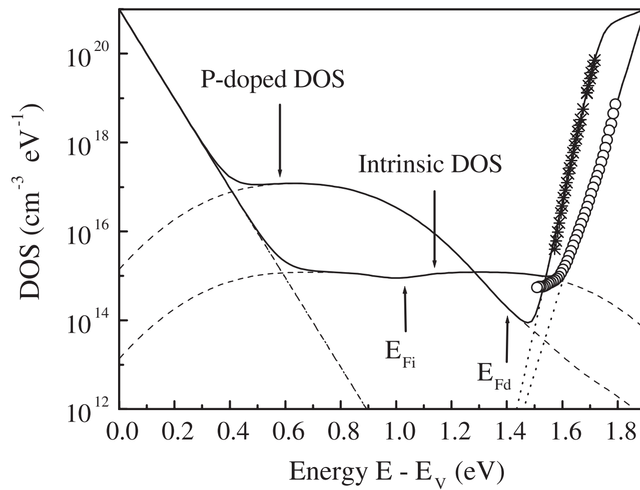

Figure 4. Complete gap DOS and its components (the conduction and valence band tail states distribution and the defect one-electron states distribution) for the intrinsic and doped cases. The conduction band tail sections determined by the TPC Fourier transform method are included. E_{Fi} and E_{Fd} denote the positions of the Fermi level in the intrinsic and doped samples, respectively.

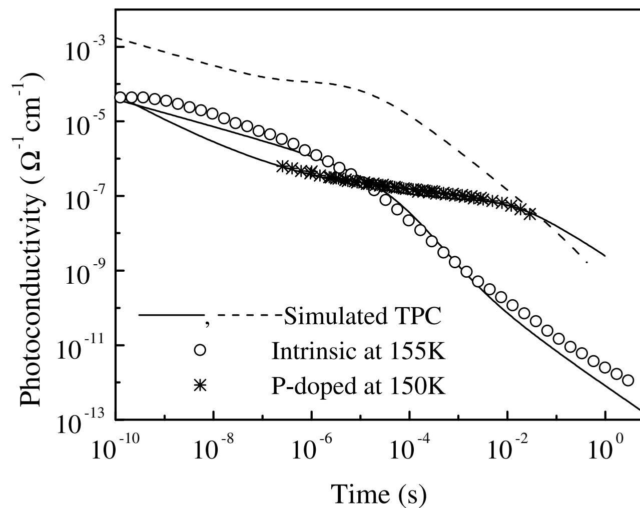

Figure 5. Simulated TPC decays (full curves) using the complete DOS models of figure 4, at 155 K for the intrinsic a-Si:H and at 150 K for the doped a-Si:H, showing good reconstruction of the experimental TPC. The broken curve is the simulated TPC for the doped case, ignoring the changes in the conduction band tail DOS due to the dopant.

The position of E_F at 0.5 eV below E_c is obtained by adding a positive dopant charge of 2×10^{16} cm^{-3} in the charge neutrality equation and taking into account the new conduction band tail distribution. The parameters used in the DPM for the valence band tail and the dangling bond DOS components are given in table 2. These reasonable parameter values give a good match between the DOS determined by the TPC Fourier transform and the DOS calculated by the DPM. Using the complete gap DOS of figure 4, they also provide a good consistent reconstruction of the original intrinsic (155 K) and doped (150 K) TPC data used

Table 2. Parameters used for the DOS calculation by the DPM.

σ (eV)	0.178
E_p (eV)	1.27
G_v (cm^{-3} eV^{-1})	10^{21}
E_{ov} (meV)	43
N_{SiSi} (cm^{-3})	2×10^{23}
H (cm^{-3})	5×10^{21}
C_{nd}^{-} (cm^3 s^{-1})	3×10^{-8}
C_{nd}^{+} (cm^3 s^{-1})	$C_{nd}^{-}/10$
C_{pd}^{+} (cm^3 s^{-1})	3×10^{-8}
C_{pd}^{-} (cm^3 s^{-1})	$C_{pd}^{+}/10$

to determine the conduction band tail profiles (figure 5). To highlight the necessity of taking into account the doping effect on the conduction band tail profile in the TPC simulation, rather than simply adding the dopant concentration in the charge neutrality equation [10], we include, in figure 5, the simulated TPC for the doped case ignoring the doping effect on the tail shape (broken curve). The latter is clearly very different from the corresponding experimental TPC.

It is worth showing, for comparison and validation, the simulated TPC curves for all temperature values and excitation densities of the experimental TPC decays given in figures 1 and 2. These are presented in figures 6 and 7 for the intrinsic and doped cases, respectively. It can be seen that all the experimental TPC features described above are reproduced, namely the short time decrease followed by the long power-law decay before recombination for the intrinsic curves and the very small slope decay before recombination for the doped curves. The shift towards longer times of the different features with decreasing temperature, and the saturation at high temperature of the initial flat region, are also verified. However, there is a temperature dependence of the parameters, especially the defect capture coefficients [17], which is not taken into account here and would prevent full reconstruction of the TPC over the full temperature range. Although this is an interesting and potentially useful observation, it is not the purpose of this paper to study this in detail, and we simply adjust the values within a reasonable range to obtain curves comparable with the experimental data. The consistency between the different DOS components, reconfirmed by the TPC simulation, should prove the occurrence of simultaneous changes in the dangling bond defect DOS and the conduction band tail DOS upon doping. Simultaneous changes in the dangling bond and the conduction band tail DOS have also been measured by Longeaud *et al* [18] in a-Si:H as the effects of light soaking and annealing.

5. Conclusions

The DOS distribution calculated by the DPM is matched to the conduction band tail DOS distribution determined by the Fourier transform of the TPC to give a complete DOS model for the TPC simulation. The TPC is simulated for intrinsic and lightly P-doped a-Si:H at different temperatures and compared to experimental TPC data. Two main points are made in this paper. Firstly, P-doping-induced changes in the conduction band tail DOS revealed by the TPC Fourier transform method are consistent with changes in the defect distribution calculated by the DPM. Secondly, the doping disorder effect on the conduction band tail profile, which gives an increased density around the donor band peak, has to be taken into account in the TPC simulation.

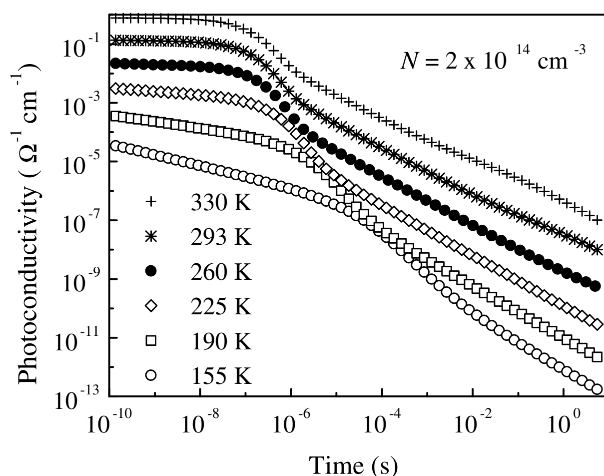

Figure 6. Simulated TPC decays for the intrinsic sample at six different temperatures (155, 190, 225, 260, 293 and 330 K) with an excitation density $N = 2 \times 10^{14}$ cm^{-3}. The curves are offset vertically for clarity.

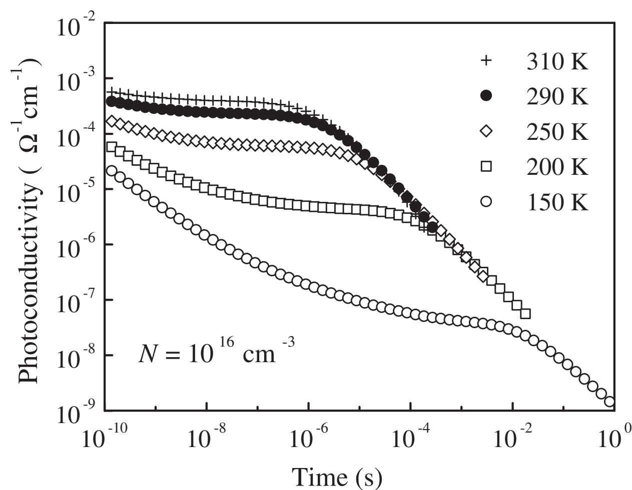

Figure 7. Simulated TPC decays for the P-doped sample at five different temperatures (150, 200, 250, 290 and 310 K) with an excitation density of $N = 10^{16}$ cm^{-3}.

Acknowledgments

The authors thank the Carnegie Laboratory group at Dundee University for the preparation of the samples. AM, AFM and AMM are grateful to the Algerian Ministry of Higher Education and Research for its support.

References

[1] Stutzmann M 1987 *Phil. Mag.* B **56** 63–70
[2] Smith Z E and Wagner S 1987 *Phys. Rev. Lett.* **59** 688–91
[3] Kakalios J, Street R A and Jackson W B 1987 *Phys. Rev. Lett.* **59** 1037–40

[4] Winer K 1990 *Phys. Rev.* B **41** 12 150–61
[5] Schumm G 1994 *Phys. Rev.* B **49** 2427–42
[6] Powell M J and Deane S C 1993 *Phys. Rev.* B **49** 10 815–27
[7] Powell M J and Deane S C 1996 *Phys. Rev.* B **53** 10 121–32
[8] Webb D P 1994 Optoelectronic properties of amorphous semiconductors *PhD Thesis* University of Abertay Dundee
[9] Main C, Brüggemann R, Webb D P and Reynolds S 1992 *Solid State Commun.* **83** 401–5
[10] Main C, Berkin J and Merazga A 1991 *New Physical Problems in Electronic Materials* ed M Borissov *et al* (Singapore: World Scientific) pp 55–86
[11] Longeaud C and Kleider J P 1993 *Phys. Rev.* B **48** 8715–41
[12] Antoniadis H and Schiff E A *Phys. Rev.* B **46** 9482–92
[13] Oheda H 1987 *J. Appl. Phys.* **62** 3803–08
[14] Main C and Reynolds S 2000 *Appl. Phys. Lett.* **76** 3085–7
[15] Street R A 1991 *Hydrogenated Amorphous Silicon* (Cambridge: Cambridge University Press) pp 150–3
[16] Merazga A, Belgacem H, Main C and Reynolds S 1999 *Solid State Commun.* **112** 535–9
[17] Yan B and Adraenssens G J 1995 *J. Appl. Phys.* **77** 5661–8
[18] Longeaud C, Roy D and Hangouan Z T 2000 *Appl. Phys. Lett.* **77** 3604–6